Exp Fluids (2010) 49:673–681
DOI 10.1007/s00348-010-0833-0

RESEARCH ARTICLE

Instability of a vertical columnar vortex in a stratified fluid

Xavier Riedinger · Patrice Meunier · Stéphane Le Dizès

Received: 23 September 2009 / Revised: 16 January 2010 / Accepted: 22 January 2010 / Published online: 17 February 2010

Abstract In this article, we study experimentally the evolution of a vertical columnar vortex in a stratified fluid. Three different measurement techniques are used. Particle image velocimetry allows us to monitor the time evolution of the characteristics of the vortex (Froude and Reynolds numbers). Dye visualizations reveal the existence of an instability for Froude numbers smaller than one, which creates an undulation of the vortex centerline. Synthetic schlieren visualization shows that the density structure of the unstable mode is very similar to the structure found recently numerically for the radiative instability of a Lamb–Oseen vortex (Riedinger et al. in J Fluid Mech, 2010). The experimental stability diagram and unstable wavelengths are compared with these numerical results. A secondary instability associated with the presence of critical layers is also observed for Froude numbers larger than one.

1 Introduction

Vortices such as the Lamb–Oseen vortex are considered as coherent structures in homogeneous fluids, but in stratified fluids they may be affected by the radiative instability as we recently found in Riedinger et al. (2010). The aim of this work is to provide an experimental evidence of such a destabilization.

Kelvin (1880) showed more than a century ago that a Rankine vortex (i.e. a patch of uniform vorticity) is stable in a homogeneous fluid with respect to 3D perturbations. However, it was shown only recently by Fabre et al. (2006) that this statement is valid for a Lamb–Oseen vortex (with a Gaussian profile of vorticity).

The effect of a stable vertical stratification was at first thought to stabilize the flow, since it prevents vertical motions. It is the case for the Kelvin–Helmholtz instability (Drazin and Reid 1981) and the centrifugal instability of a Taylor–Couette flow (Withjack and Chen 1974). But the stratification can also lead to new instabilities such as the zig-zag instability of a vortex pair (Billant and Chomaz 2000a, b) and the tilt-induced instability of a non-vertical vortex (Cariteau 2005; Boulanger et al. 2008). It was also recently shown numerically (Yavneh et al. 2001; Molemaker et al. 2001) and experimentally (Le Bars and Le Gal 2007) that the stratification can destabilize the Taylor-Couette flow in centrifugally stable regions of the parameter space. This strato-rotational instability is associated with a phenomenon of resonance of neutral boundary modes (Yavneh et al. 2001; Le Dizès and Riedinger 2010).

In the absence of boundaries, Ford (1994) discovered that a Rankine-like vortex is unstable in rotating shallow water, by a mechanism of internal gravity wave emission. This result was further extended for continuously stratified flows by Schecter and Montgomery (2004) and Billant and Le Dizès (2010). A similar result was also obtained by Plougonven and Zeitlin (2002) in a slightly different framework. Le Dizès and Billant (2009) analyzed the mechanism of instability for arbitrary vortices using a "Wentzel–Kramers–Brillouin–Jeffreys" (WKBJ) approach and obtained inviscid growth rate estimates for a Gaussian vortex. These results were extended numerically in Riedinger et al. (2010) for a large range of Reynolds numbers and Froude numbers. In this paper, it was shown that the most unstable mode is a helicoidal mode with a small frequency, which is often called slow bending wave

X. Riedinger (✉) · P. Meunier · S. Le Dizès
IRPHE, CNRS & Aix-Marseille University,
49, Rue F. Joliot Curie, 13013 Marseille, France

(Leibovich et al. 1986) or displacement mode, since it translates the vortex filament as a whole. The goal of this paper is to observe such an unstable mode in a controlled experiment. The experimental set-up is described first in Sect. 2.1. We show that it allows us to generate a single vortex, which is characterized in Sect. 2.2. The description of the instability is performed in Sect. 3, using both visualization and schlieren techniques. The comparison with the numerical results is done in Sect. 3.3. The case of large Froude numbers for which the instability disappears is treated in Sect. 3.4. A summary of the results is finally provided in Sect. 4.

2 Generation of a solitary vortex

In this section, we describe the apparatus that is used to create a single laminar vortex in a stratified fluid. Such an apparatus has already been used in previous studies (Cariteau and Flór 2006; Boulanger et al. 2007). A particular effort is made here to minimize the influence of other distant vortices.

2.1 Experimental set-up

The experimental set-up is presented in Fig. 1. Experiments are performed in a 1.50-m long, 0.75-m wide and 0.50-m high Plexiglass tank, which is filled with a stratified fluid. The stratification is established by the two-tank method, using fresh water in the first tank and salted water with a density of 1,190 kg m^{-3} in the second tank. Two stratifications are considered: a moderately strong linear stratification over a height of 45 cm (leading to a Brunt-Väisälä frequency $N = \sqrt{-g\partial_z\rho/\rho_0} = 2.09$ rad s^{-1}) and a strong stratification over a height of 20 cm (leading to $N = 2.96$ rad s^{-1}). For the strong stratification, the linearly stratified layer lies in between a top layer of 10 cm of fresh water and a bottom layer of 15 cm of salted water, in order to minimize boundary effects associated with the free surface and the bottom of the tank.

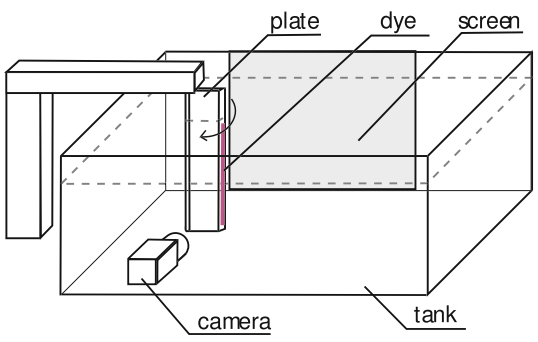

Fig. 1 Experimental setup used for the generation of the solitary vortex. The camera records the position of the dye (for visualizations) and the deformation of the screen (for Synthetic Schlieren)

The vortex is created by rotating impulsively a flap (visible in Fig. 1) in the fluid initially at rest. The rotation is performed by a computer-controlled step-motor. This method has been used frequently in other studies (see Thomas and Auerbach 1994; Cariteau 2005; Boulanger et al. 2007) and is known to create a very laminar vortex. However, this technique usually creates a stopping vortex during the deceleration phase of motion of the plate, which may interfere with the dynamics of the main vortex. To minimize this effect, which can become important for long times ($t > 120$s), we had to modify the experiment. In particular, the dimension of the plate was chosen larger than in previous experiments: we used a 30-cm wide flap instead of a 10-cm wide flap, such that the distance between vortices is increased. Then, the motion of the flap has been chosen carefully in order to minimize the circulation of the stopping vortex. Starting from the motion used in Boulanger et al. (2007), the law of motion has been progressively modified and improved using particle image velocimetry (PIV) measurements in a horizontal plane. The motion law finally adopted for the angle θ of the plate (in radians) is:

$$0 < \theta < 0.94 : \dot{\theta} = \dot{\Theta}_{\max} \frac{0.2164}{\theta + 0.0175} \left\{ 1 - e^{-\left(\frac{\theta}{0.1222}\right)^{5/4}} \right\} \quad (1)$$

$$0.94 < \theta < 1.40 : \dot{\theta} = \dot{\Theta}_{\max} 0.00403(110 - \theta). \quad (2)$$

Figure 2 shows the resulting angular velocity $\dot{\theta}$ of the plate as a function of the angle and as a function of time. The motion consists of a rapid acceleration followed by a gradual slow-down up to the angle $\theta = 1.40$ rad (corresponding to 80°). This law is optimized to create a nearly Gaussian vortex and to avoid other parasitic counter-rotating vortices up to a distance of 10 cm from the primary vortex, as will be shown in the next section. The circulation of the vortex is varied by modifying the maximal angular velocity $\dot{\Theta}_{\max}$ between 0.02 and 0.09 rad s^{-1}.

Particle image velocimetry measurements have been done in a horizontal section at mid-height of the vortex. For this purpose, the fluid has been homogeneously seeded with small reflecting particles of diameter 10 μm (Spheriçel hollow glass spheres 110P8 from Potter Industries) illuminated by a 3–5-mm thick laser sheet produced by a 170-mJ pulsed ND-Yag laser (Quantel). The density of the particles is peaked around 1.1 kg m^{-3} and is distributed between 1 and 1.2 kg m^{-3}, i.e. on the range of densities of the stratified fluid. They are introduced at the depth of the laser sheet and diffuse in approximately 1 day on the whole height of the tank. Image pairs are recorded by a digital

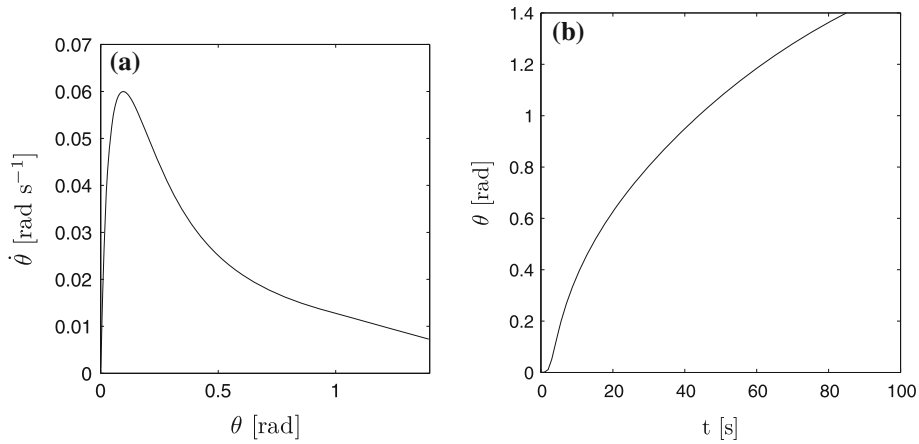

Fig. 2 Description of the motion of the flat plate generating the vortex for a maximal velocity $\dot{\Theta}_{max} = 0.06$ rad s^{-1}. **a** Angular velocity of the flap $\dot{\theta}$ as a function of its angle θ. **b** Temporal evolution of the angle θ of the flap

PIV camera (Roper Megaplus ES 4.0) triggered by the laser pulses. The time interval between two PIV exposures is 20 or 40 ms. The time between two image pairs is 1 s, which makes the data time-resolved because the flow evolves slowly (over 40-80 s). The images are treated by an in-house cross-correlation algorithm (Meunier and Leweke 2003). The accuracy of the PIV software is 0.1 pixel on the displacement of the particles between the two images (Meunier and Leweke 2003). This makes the relative error on the velocity of the order of 2%, since the time interval is chosen such that the mean displacement is of the order of five pixels. More details on the PIV technique are given in Boulanger et al. (2007).

The evolution of the vortex is measured through dye visualizations. As showed on Fig. 1, Rhodamine B dye mixed with water and a silicone paste (to make it thicker) is painted on the edge of the plate, when the plate is above the water. After the dye is dry, the flap is slowly immersed. The disturbances created in the fluid are weak and have totally disappeared after 5 min when the flap is moved. The generation of the vortex creates a sheet of magenta dye, which detaches from the edge of the flap and rolls up around the vortex core. It is very efficient to obtain side views of the vortex as a function of time. Images are recorded using a Nikon camera D200 with a lens of 50 mm. As for PIV measurements, the frame rate of dye visualizations and synthetic schlieren visualizations is 1 Hz.

Synthetic schlieren visualizations are made using the method described in Sutherland et al. (1999). With this purpose, a screen printed with black and white little dots is pasted on the back of the tank (see Fig. 1). A digital camera (Nikon D200) records images of the screen through the tank during the experiment. The presence of density gradients in the fluid contained in the tank creates deviations of the light rays, since the refraction index is proportional to the density gradient. Comparing the position of the dots in the presence and in the absence of density gradients gives a 2D field of the density gradient integrated along the width of the tank. Different properties of the vortex can thus be visualized, by looking at the vertical or horizontal component of the density gradient. The algorithm used to treat the images is a modified version of the PIV algorithm. These synthetic schlieren visualizations can be made simultaneously to the dye visualizations by treating only the red component of the digital pictures, since the dye is not visible in this component when the background is white.

2.2 Vortex characteristics

Figure 3a shows a typical vorticity field obtained by PIV measurements in a horizontal plane at mid-height of the vortex. We can clearly identify an axisymmetric vortex, which was created by a rotation of the flat plate (visible as the thick black line). The vortex is almost motionless: it moves with a velocity ten times smaller than the velocity of the plate. It can be noted that there is no stopping vortex with a vorticity larger than 0.4 s^{-1} (i.e. 10% of the maximum vorticity of the primary vortex). In fact, there is a weak stopping vortex, located at $x = -7$ cm and $y = -7$ cm, i.e. 15 cm far from the primary vortex, and its circulation was measured to be 10 times smaller than the circulation of the primary vortex. This ensures that the interaction of the primary vortex with possible stopping vortices is weak enough, such that no elliptic or zig-zag instabilities are present. In particular, our velocity field is different from the field obtained by Cariteau and Flór (2006) where the elliptic instability was the dominant dynamical feature.

Figure 3b presents the radial profile of the mean azimuthal velocity v_θ. It is very well approximated by the profile of a Gaussian vortex (Lamb–Oseen), whose azimuthal velocity is given by:

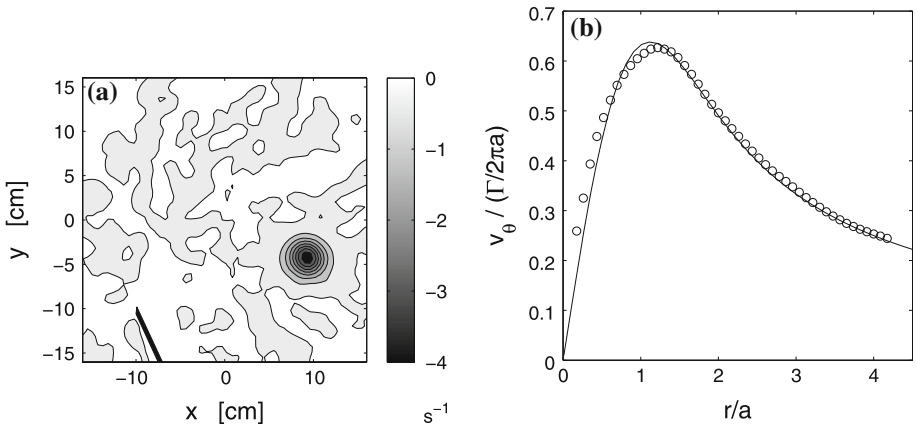

Fig. 3 Description of the base flow for $\dot{\Theta}_{max} = 0.06$ rad s^{-1} at $t = 40$ s. **a** PIV vorticity field of the vortex. The plate is showed as a *black line in the bottom left corner*. **b** Mean azimuthal velocity profile of the vortex, obtained experimentally (*open circle*) and by a fit (*solid line*) with a Gaussian profile defined by (3)

$$v_\theta(r) = \frac{\Gamma}{2\pi r}(1 - e^{-r^2/a^2}). \tag{3}$$

This expression is used in a Matlab© program to make a least-square fit of the vorticity field, in order to obtain the evolution of the circulation Γ and of the core size a. This procedure is very accurate for the circulation with an uncertainty of 2%, but is less accurate for the core size, with an uncertainty of the order of 5%, leading to an uncertainty of 12% on the timescale $2\pi a^2/\Gamma$. The results of this fitting for $\dot{\Theta}_{max} = 0.06$ rad s^{-1} are given in Fig. 4a and b. After the creation of the vortex (between $t = 0$ s and $t = 10$ s), the circulation remains approximately constant (within 5%): here, $\Gamma = 48$ cm^2 s^{-1}. By redoing the experiment with a different angular velocity of the plate, we found that the circulation is proportional to the maximum angular velocity $\dot{\Theta}_{max}$ of the plate and is fairly independent of the stratification and of the viscosity. This leads to an empirical formula for the circulation of the vortex $\Gamma = 769\dot{\Theta}_{max}$, if $\dot{\Theta}_{max}$ is given in rad s^{-1} and Γ is in cm^2 s^{-1}.

By contrast, the core size increases in time owing to the viscous diffusion of vorticity. The square of the core size a^2 increases linearly during the first 40 s, which is in agreement with the evolution of the Gaussian vortex radius:

$$a^2 = a_0^2 + 4\nu t \tag{4}$$

where $\nu = 0.0102$ cm^2 s^{-1} is the viscosity of the fluid. After 40 s, the square of the core size increases faster due to the presence of the instability, which will be described in the next section. Considering all PIV experiments, we notice that the initial core size a_0 is independent of the angular velocity $\dot{\Theta}_{max}$ of the plate and of the stratification (within the noise in the measurement) and is equal approximatively to $a_0 = 1.22$ cm.

Now that the 2D velocity field of the vortex is correctly known, we can define the non-dimensional parameters of this base flow, which are the Reynolds number and the Froude number. The Reynolds number is easily defined as

$$Re = \frac{\Gamma}{2\pi\nu} \tag{5}$$

and is almost independent of time as soon as the vortex is created ($t > 15$ s in Fig. 4a). However, the horizontal Froude number, which is defined as

$$F = \frac{\Gamma}{2\pi N a^2} \tag{6}$$

depends on time, since the core size a of the vortex increases with time. The Froude number thus decreases

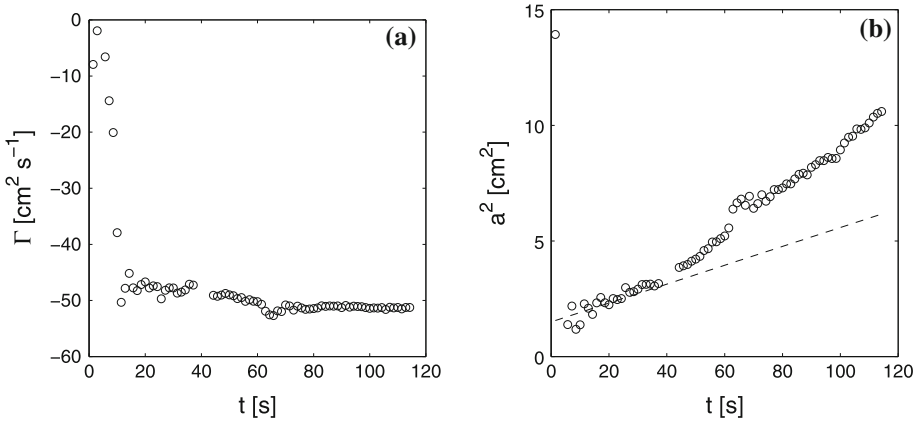

Fig. 4 Temporal evolution of the circulation (**a**) and of the square of the core size (**b**) of the vortex for $\dot{\Theta}_{max} = 0.06$ rad s^{-1}. Symbols are obtained from a 2D least-square fitting of the PIV velocity fields. The *dashed line* shows the viscous evolution (4) for a Gaussian vortex

with time for each experiment. For example, in an experiment with $N = 2.09$ rad s^{-1}, the Froude number decreases from $F = 1.5$ at $t = 20$ s to $F = 0.9$ at $t = 60$ s. This effect makes it difficult to compare the experimental results with the numerical stability analysis obtained for a frozen Lamb–Oseen vortex, that is for $a =$ constant (Riedinger et al. 2010). On the other hand, the time at which the instability is observed gives a lower estimate of the Froude number below which the flow becomes unstable.

3 Instability of a vertical stratified vortex

3.1 Dye visualization of a destabilization

Figure 5 shows a side view of the temporal evolution of the vortex during an experiment, using the dye visualization technique. At $t = 0$ s, the plate starts to move toward the observer. At $t = 10$ s, the plate (still visible on the left of the picture) has created a straight line of dye, which has detached from the plate and marks the core of the vortex. Between $t = 20$s and $t = 40$ s, the line of dye starts to undulate, with an amplitude that grows very slowly in time. Although this undulation remains weak, it is reproducible: the time at which it appears and the wavelength do not vary much from one experiment to the other, which proves that it is not linked to residual motions in the tank. Moreover, for the strong stratification case (for which the stratified fluid column is sandwiched between two large homogeneous layers), the undulation of the vortex is visible only in the stratified layer. This shows that this instability is associated with the presence of the stratification. At $t = 50$ s and $t = 60$ s, the growth of the undulation stops and the deformation is not sinusoidal anymore, probably due to the presence of harmonics. In most cases, the dye line forms in fact a helical shape at late stages, although it is not visible on these 2D photographs.

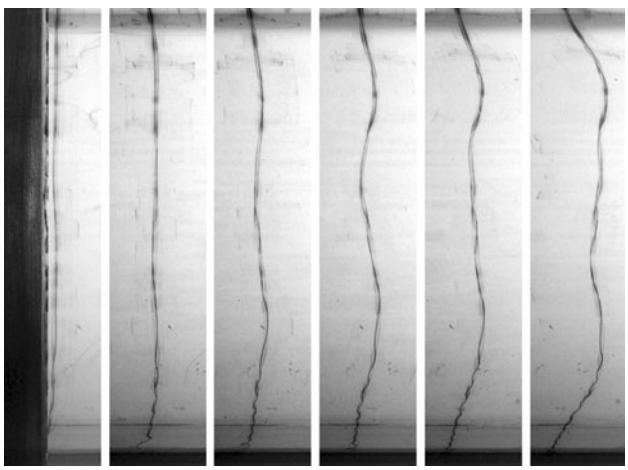

Fig. 5 Dye visualization of the destabilization of the columnar vortex for $Re = 480$ and $N = 2.09$ rad s^{-1}. The sideview images are taken at $t = 10/20/30/40/50/60s$. The field of the view is approximately 45 cm in height

This deformation is the consequence of a weak destabilization of the columnar vortex flow occurring in the core. This structure is similar to the typical deformation due to a displacement mode, also called "slow bending waves" (Leibovich et al. 1986). This mode can become unstable due to the interaction of several vortices in a homogeneous fluid (Crow 1970) and in a stratified fluid (Billant and Chomaz 2000a). It is striking to see that this mode is unstable, even in the absence of a second vortex. However, the growth rate is much smaller here than for the zig-zag instability and it saturates at a lower amplitude.

The wavelength of the undulation and the time of onset of the instability are measured for each Reynolds number and for the two stratifications that we have considered. The results are compiled in Table 3.1 for a Reynolds number varying from 360 to 960. For Reynolds numbers larger than 960, the vortex remains straight but the dye mark creates a cloudy pattern, indicating that the vortex is turbulent. For Reynolds numbers smaller than 360, the initial undulation of the vortex does not grow in time. The wavelength seems to be slightly increasing with the Reynolds number, but the measurement of the wavelength is not very accurate, since the deformation is weak and not perfectly sinusoidal. The uncertainty is found to be of the order of 15% for the wavelength. The time of onset of the instability seems also to be increasing with the Reynolds number. This is surprising because we would expect the instability to grow faster at larger Reynolds numbers (Table 1). We will see in Sect. 3.3 that it is in fact an effect of the Froude number. The uncertainty on the time of onset is of the order of 10 s.

3.2 Synthetic schlieren visualization

Synthetic schlieren measurements were done simultaneously with the dye visualizations. An example of the horizontal density gradient $\partial\rho/\partial x$ is shown as pseudo-colors in Fig. 6a at time $t = 54$ s and for $Re = 600$. The dye is superimposed in black to the density gradient. The grey area on the left of the image corresponds to the flat plate. It is clear that the core of the vortex contains a sinusoidal perturbation of the density gradient in the vertical direction. This perturbation is in phase quadrature with the undulation of the vortex: the density gradient is maximum or minimum (red or blue) between two peaks of the undulation of the vortex centerline and not at a peak of the undulation. This is exactly what is expected for a displacement mode because the vorticity and the density are in phase quadrature.

Table 1 Experimental parameters used for the different runs

$\dot{\Theta}_{max}$(rad s^{-1})	Γ (cm^2 s^{-1})	*Re*	$F(t=0)$	$F(t_i)$	λ(cm)	t_i(s)	a_i(cm)
$N = 2.09$ rad s^{-1}							
0.03	23.1	360	1.18	0.67	9.1	28	1.62
0.03	23.1	360	1.18	0.7	21	25	1.58
0.04	30.8	480	1.57	0.86	18	30	1.65
0.05	38.4	600	1.97	0.94	14.6	40	1.77
0.05	38.4	600	1.97	0.77	16.8	57	1.95
0.06	46.1	720	2.36	1.12	20.9	40	1.77
0.07	53.8	840	2.75	1.04	16.8	60	1.98
0.07	53.8	840	2.75	1.16	20.5	50	1.88
0.08	61.5	960	3.15	1.19	21.7	60	1.98
$N = 2.96$ rad s^{-1}							
0.03	23.1	360	0.83	0.37	8.34	18	1.49
0.04	30.8	480	1.11	0.50	9.2	35	1.71
0.05	38.4	600	1.39	0.62	9.2	40	1.77
0.06	46.1	720	1.67	0.75	9.7	40	1.77
0.07	53.8	840	1.94	0.87	9.4	50	1.88
0.08	61.5	960	2.22	1	12	50	1.88

Wavelengths and instant of appearance of the undulation obtained from dye visualization are also reported. The same angular velocity may appear twice, meaning that the experiment has been done twice

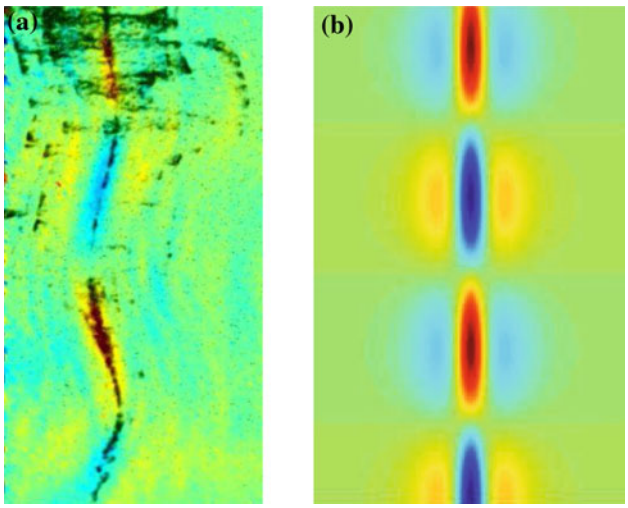

Fig. 6 **a** Dye and synthetic schlieren visualizations of the instability superimposed. Dark color corresponds to the dye and red (resp. blue) color corresponds to positive (resp. negative) horizontal density gradient. $N = 2.09$ rad s^{-1}, $t = 54$ s, ($Re = 600$, $F = 0.79$). **b** Horizontal density gradient obtained numerically for the displacement mode at the same Froude and Reynolds number. The height of the field of view is 34 cm

It can be noted that each central band of negative (resp. positive) density gradient is surrounded by two bands of positive (resp. negative) density gradient on each side. This structure is once again in agreement with the structure of a displacement mode, which is shown in Fig. 6b. It was calculated numerically using the linear stability code of Riedinger et al. (2010) at the same wavelength and Froude number. The structure also corresponds to the isodensity deformations of a tilted vortex because of the hydrostatic equilibrium.

In this paper, we have shown that the displacement mode also exhibits a spiral internal gravity wave structure far from the vortex. However, the density gradient associated with these internal waves far from the vortex is close to zero as the radiated waves are almost horizontal. So we have not been able to measure this wave structure. Some internal waves have been observed inside the tank by looking at the vertical density gradient. But they do not seem to be related to the dynamics of the main vortex as they are generated at the lower corner of the flat plate during the creation of the vortex.

3.3 A radiative instability

We now try to understand why the undulation grows in time. A first explanation would be that the bending of the vortex is due to viscous effects at the bottom of the tank. But the deformation would then be localized at the bottom of the vortex and would not create a sinusoidal undulation with two wavelengths affecting the whole vortex. We did observe some deformations associated with boundary effects for small Reynolds numbers but it could always be differentiated from the growth of the vortex undulation which, in our mind, is due to an instability.

In a stratified fluid, a vortex is known to be affected by the so-called zig-zag instability when it is surrounded by other vortices. In our first experiments when the motion of the plate was not sufficiently optimized to avoid the formation of a close stopping vortex, we did observe such an instability. It was clear in the schlieren visualizations, but the perturbation was mainly centered on the stopping vortex and not on the main vortex. A growth of the perturbation on the main vortex was observed, but it occurred clearly after the perturbation of the stopping vortex. After optimization of the plate motion, we only observed a unique perturbation, always centered on the primary vortex. This was checked by simultaneous use of synthetic schlieren and dye visualization. We therefore think that this perturbation is not due to any trace of surrounding vorticity but is instead the evidence of the radiative instability we recently predicted (Riedinger et al. 2010). This instability has been shown to affect solitary Gaussian vortices placed in stratified environment. It can excite various modes, but the most unstable mode for $Re < 1000$ is the displacement mode whose structure is in agreement with the experimental observation. The numerical results are summarized in Fig. 7, which shows the maximum non-dimensional

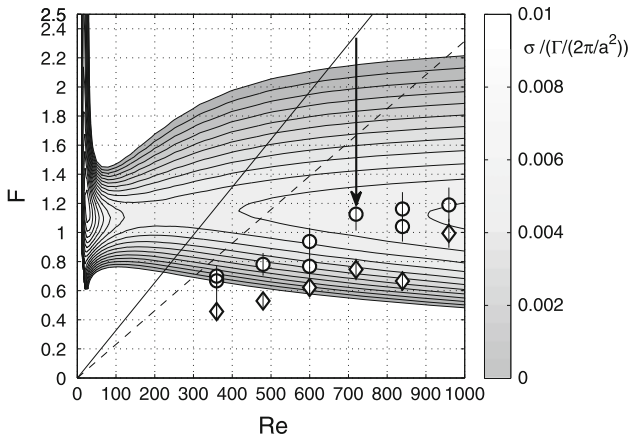

Fig. 7 Stability diagram of the radiative instability. Grey scale levels correspond to the non-dimensionalized (using the maximal angular velocity) growth rate of the instability found numerically for a Gaussian vortex (Lamb–Oseen vortex). *Symbols* indicate the parameters at which the instability is observed experimentally for $N = 2.09$ rad s^{-1} (*open circle*) and for $N = 2.96$ rad s^{-1} (*open diamond*). The *arrow* shows the temporal evolution of the Froude number during an experiment. The *solid* (resp. *dashed*) line gives the Froude number at the beginning of the experiment for $N = 2.09$ rad s^{-1} (resp. $N = 2.96$ rad s^{-1})

growth rate $\sigma/(\Gamma/(2\pi a^2))$ of the radiative instability as a function of Froude and Reynolds number. The unstable band is centered around $F = 1$, which approximately corresponds to the experimental conditions. The growth rate remains weak (<1% of the maximal angular velocity of the vortex), which explains the slow growth of the undulation in our experiments. To provide a more quantitative comparison between experiments and theory, we have indicated with symbols on Fig. 7 the Froude and Reynolds numbers at the time of onset of the instability. Almost all unstable experiments fall into the unstable domain, although they are mainly localized below the most unstable Froude number. We have to recall that for each experiment, the Reynolds number is fixed, but the Froude number slowly decreases in time (as indicated by the arrow), starting from an initial value located on the black line. This could explain why the instability is visualized for Froude numbers smaller than the most unstable Froude number, because the Froude number has decreased by the time the undulation has become visible. However, it would be difficult to quantify the delay in the observation of the undulation because it depends on the initial turbulence in the tank before the experiment and on the orientation of the plane of the undulation. This also explains why the instability appears later at higher Reynolds numbers: the vortex reaches the unstable domain later because its initial Froude number is higher.

In Fig. 8, we plot the wavelengths λ measured in the experiment in dimensional units. The observed wavelength always falls within the unstable band predicted numerically (indicated as a grey area) except at low Reynolds numbers where the growth rate of the instability was extremely small. However, the observed wavelength is always larger than the most unstable wavelength predicted numerically (shown as solid lines). The discrepancy is small for the strongest stratification (30%) but it is rather large for the weakest stratification (by a factor two). This is not surprising because the dimensional growth rate is smaller for the weakest stratification. Indeed, the dimensional growth rate is of order $\sigma \approx 0.01\Gamma/(2\pi a^2)$ in the most unstable region (i.e. where $F = \Gamma/(2\pi N a^2) \approx 1$), which leads to $\sigma \approx 0.01\,N$. It could be argued that the discrepancy comes from the variation of the core size a and of the Froude number in time which gives $\lambda = \lambda_{\mathrm{nd}}(F(t))a(t)$, where $\lambda_{\mathrm{nd}}(F)$ is the most unstable non-dimensional wavelength obtained with the numerical code at a specific Froude number F. But the two effects in fact balance each other and lead to a very weak variation in the most unstable wavelength. Indeed, we show numerically in Fig. 9 that it varies by <15% during the first minute of the experiment. However, even if the most unstable wavelength remains constant, the structure of the unstable mode evolves during the experiment and it might be less sensitive to the change of a and F at large wavelengths than at small wavelengths. This could explain the discrepancy.

3.4 Influence of a critical layer for $F > 1$

We have observed a different structure at the beginning of the experiments, for moderate and large Reynolds numbers when $F > 1$. This structure exhibits two thin vertical layers of opposite sign density gradient (red and blue) on each side of the vortex core. They can be distinguished in the upper part of Fig. 10a. These vertical bands appear for high enough Froude numbers and always merge toward the center before disappearing when the Froude number becomes smaller than one. They are probably related to a critical layer which appears in the displacement modes for $F > 1$ (Riedinger et al. 2010) and which was also observed in the dynamics of a tilted vortex (Boulanger et al. 2007). Indeed as soon as $F > 1$, the small frequency displacement mode is known to possess a critical radius where the angular velocity of the vortex is equal to the Brunt-Väisälä frequency. At this critical radius, the vertical forcing created by the displacement mode (or by tilting for a tilted vortex) is in resonance with the Brunt-Väisälä frequency, which generates a theoretical divergence of the vertical velocity and of the density. In the linear regime, this critical layer is responsible for the damping of the mode for large Froude numbers. In the experiments, the flow in the critical layer becomes nonlinear and saturates. Due to the variation of the Froude number, the critical radius moves

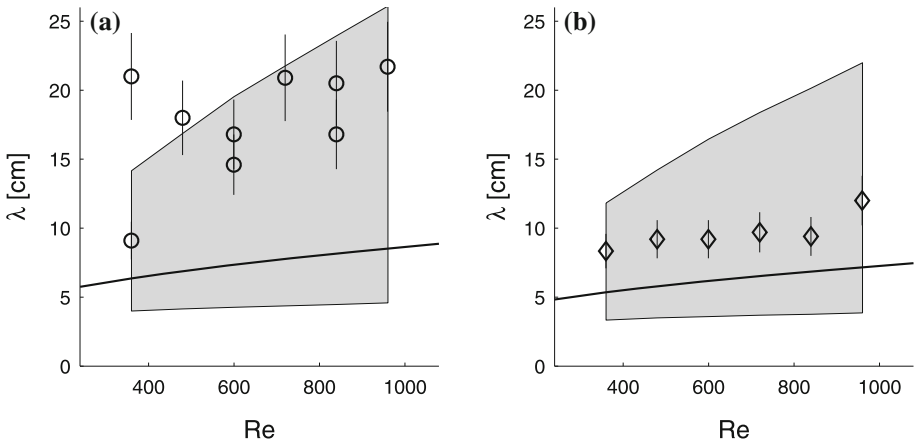

Fig. 8 Variation of the dimensional wavelengths with the Reynolds number. Symbols correspond to experimental measurements. Numerical results are used to predict the unstable band of wavelengths for $F = 1$ (*grey area*) and the most unstable wavelength along time (*solid line*).
a $N = 2.09$ rad s^{-1},
b $N = 2.96$ rad s^{-1}

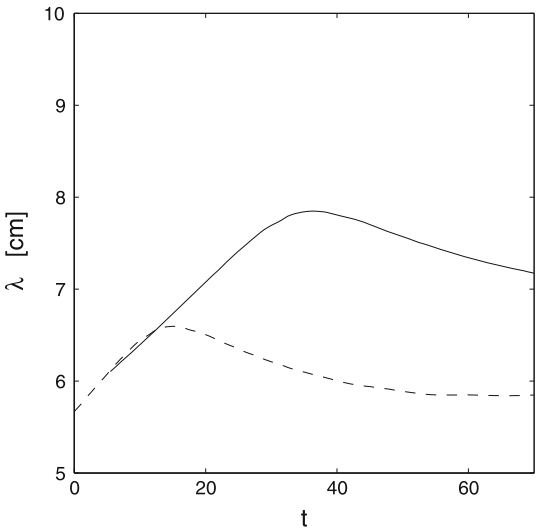

Fig. 9 Temporal evolution of the most unstable wavelength, predicted numerically for two stratifications: $N = 2.09$ rad s^{-1} (*solid line*) and $N = 2.96$ rad s^{-1} (*dashed line*). $Re = 720$

inward during the experiment and disappears when $F < 1$. We suspect that the saturation of the flow in the critical layer could delay the observation of the displacement mode associated with the primary instability until the Froude number gets smaller than one.

Otherwise, in the nonlinear regime, the critical layer can also exhibit a different dynamic. In Boulanger et al. (2008), it was shown that the strong shear that is created in the critical layer can lead to a violent 3D instability when the tilt angle of the vortex (which is here equivalent to the amplitude of the displacement mode) is larger than $Re^{-2/3}$. In our mind, the horizontal lines of alternate density gradients visible in Fig. 10b are the trace of such a secondary instability. The small scale structures are organized in bands and are present only for Reynolds numbers larger than 960. We do not observe them in the experiments presented in Figs. 7 and 8.

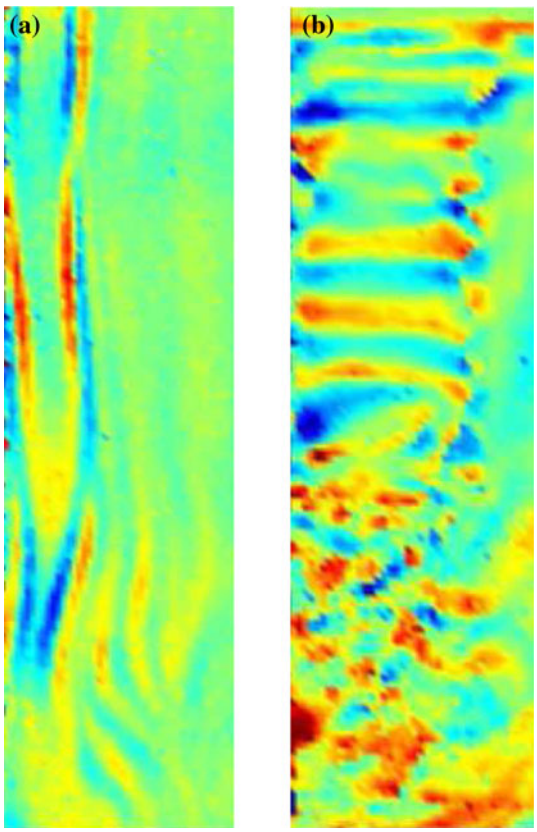

Fig. 10 Schlieren visualization of the critical layer obtained for $F > 1$ (**a**) and of its instability (**b**). Pseudo-colors correspond to the horizontal (**a**) and vertical (**b**) density gradient. **a** $Re = 600$, $N = 2.09$ rad s^{-1}, $t = 29$ s. **b** $Re = 1080$, $N = 1.6$, $t = 25$s

4 Conclusion

We have studied the evolution of columnar vortices for Reynolds numbers <1,000 and for moderate Froude numbers in the range 0.2–2. Special attention has been paid to create a single vortex, far from any other surrounding vortex. This has allowed us to visualize for the first time the radiative instability of a solitary vertical vortex in a

stratified fluid, which was theoretically predicted in Riedinger et al. (2010). Dye visualizations and synthetic schlieren visualizations have shown that it consists of a displacement mode (or slow bending wave) as predicted by the theory. The measured wavelength was found larger than the most unstable wavelength predicted by the theory but still within the theoretical instability band. Synthetic schlieren visualizations have also revealed the presence of a critical layer for Froude numbers larger than one which could delay the undulation induced by the displacement mode or be responsible of a secondary instability analogous to the tilt-induced instability (Boulanger et al. 2008).

These results settle on the first experimental evidence that a Gaussian vortex, which is known to be stable in a homogeneous fluid can be destabilized in the presence of stratification. This may have important consequences in geophysical applications. Indeed, the small-scale atmospheric cyclones can have Froude numbers of the order of unity and large Rossby numbers and therefore be subject to the radiative instability. Moreover, oceanic vortices shedded behind coastal capes or promontories might also be unstable via this mechanism. However, the growth rate of this instability is weak so it is not clear whether this instability will have time to develop in an evolving flow. This instability is nevertheless a source of internal gravity waves, which perhaps deserves to be considered in the modeling of the upper atmosphere.

References

Billant P, Chomaz JM (2000a) Experimental evidence for a new instability of a vertical columnar vortex pair in a strongly stratified fluid. J Fluid Mech 418:167–188

Billant P, Chomaz JM (2000b) Theoretical analysis of the zigzag instability of a columnar vortex pair in a strongly stratified fluid. J Fluid Mech 419:29–63

Billant P, Le Dizès S (2009) Waves on a columnar vortex in a strongly stratified fluid. Phys Fluids 21 (106602)

Boulanger N, Meunier P, Le Dizès S (2007) Structure of a tilted stratified vortex. J Fluid Mech 583:443–458

Boulanger N, Meunier P, Le Dizès S (2008) Instability of a tilted vortex in stratified fluid. J Fluid Mech 596:1–20

Cariteau B (2005) Etude de la stabilité et de l'interaction de cyclones intenses en fluide stratifié. PhD thesis, Université Joseph Fourier, Grenoble

Cariteau B, Flór JB (2006) An experimental investigation on elliptical instability of a strongly asymmetric vortex pair in a stable density stratification. Nonlin Processes Geophys 13:1–9

Crow SC (1970) Stability theory for a pair of trailing vortices. AIAA J 8(12):2172–2179

Drazin PG, Reid WH (1981) Hydrodynamic stability. Cambridge University Press, Cambridge

Fabre D, Sipp D, Jacquin L (2006) The Kelvin waves and the singular modes of the Lamb-Oseen vortex. J Fluid Mech 551:235–274

Ford R (1994) The instability of an axisymmetric vortex with monotonic potential vorticity in rotating shallow water. J Fluid Mech 280:303–334

Kelvin L (1880) Vibrations of a columnar vortex. Phil Mag 10:155–168

Le Bars M, Le Gal P (2007) Experimental analysis of the stratorotational instability in a cylindrical Couette flow. Phys Rev Lett 99 (064502)

Le Dizès S, Billant P (2009) Radiative instability in stratified vortices. Phys Fluids 21 (096602)

Le Dizès S, Riedinger X (2010) The strato-rotational instability of keplerian and Taylor-Couette flows. J Fluid Mech (submitted)

Leibovich S, Brown S, Patel Y (1986) Bending waves on inviscid columnar vortices. J Fluid Mech 173:595–624

Meunier P, Leweke T (2003) Analysis and optimization of the error caused by high velocity gradients in particle image velocimetry. Exp Fluids 35(5):408–421

Molemaker MJ, McWilliams JC, Yavneh I (2001) Instability and equilibration of centrifugally stable stratified Taylor-Couette flow. Phys Rev Lett 86:5270–5273

Plougonven R, Zeitlin V (2002) Internal gravity wave emission from a pancake vortex: an example of wave-vortex interaction in strongly stratified flows. Phys Fluids 14:1259–1268

Riedinger X, Le Dizès S, Meunier P (2010) Viscous stability properties of a Lamb-Oseen vortex in a stratified fluid. J Fluid Mech (in press)

Schecter DA, Montgomery MT (2004) Damping and pumping of a vortex Rossby wave in a monotonic cyclone: critical layer stirring versus inertia–buoyancy wave emission. Phys Fluids 16:1334–1348

Sutherland BR, Dalziel SB, Hughes GO, Linden PF (1999) Visualization and measurement of internal waves by 'synthetic schlieren'. Part 1. Vertically oscillating cylinder. J Fluid Mech 390:93–126

Thomas P, Auerbach D (1994) The observation of the simultaneous development of a long and short-wave instability mode on a vortex pair. J Fluid Mech 265:289–302

Withjack E, Chen C (1974) An experimental study of Couette instability of stratified fluids. J Fluid Mech 66:725–737

Yavneh I, McWilliams J, Molemaker M (2001) Non-axisymmetric instability of centrifugally stable stratified Taylor–Couette flow,. J Fluid Mech 448:1–21